

Electronic Supplementary Information

Highly Efficient Oxygen Photosensitization of Carbon dots: the Role of Nitrogen Doping

Shihong Wu,^{a, b} Ronghui Zhou,^c Hanjiao Chen,^b Jinyi Zhang,^b Peng Wu^{*, a, b}

[†]State Key Laboratory of Hydraulics and Mountain River Engineering, Sichuan University, Chengdu 610065, China

[‡]Analytical & Testing Center, Sichuan University, Chengdu 610064, China

[‡]State Key Laboratory of Oral Diseases, West China Hospital of Stomatology, Sichuan University, Chengdu 610041, China

Corresponding author's E-mail: wupeng@scu.edu.cn

Apparatus

All the instrumental information used for characterizations were given in Table S1.

Table S1. The instrumental information used for characterizations in this work.

Characterization items	Instrument model	Manufacturer
UV/Vis absorption spectra	Lambda-365 spectrometer	Perkin Elmer, USA
Fluorescence & Phosphorescence	FluoroMax-4P spectrofluorometer	Horiba Scientific, USA
Fluorescence & Phosphorescence	Fluolog-3 spectrofluorometer	Horiba Jobin Yvon, USA
lifetime & $^1\text{O}_2$ emission	Phosphorescence lifetime excitation: Spectra LED (355 nm, S-355,) Fluorescence lifetime excitation: DeltaDiode (371 nm, DD-375L)	
Fluorescence quantum yield	Fluolog-3 spectrofluorometer with an integration sphere (IS80, Labsphere)	Horiba Jobin Yvon, USA
EPR	EMX plus-10/12	Bruker, Switzerland
XPS	AXIS Ultra DLD 800 X (Excitation: Al-K α X-ray)	Kratos, UK
FT-IR	Nicolet iS10	Thermo Scientific, USA
Raman	LabRAM HR800	Horiba Jobin Yvon, France
Zeta potential	Zetasizer Nano ZS	Malvern, England
Vitro cytotoxicity	Varioskan Flash	Thermo Fisher Scientific, USA
ROS detection	Fluorescent Inverted Microscopy	Leica DMI8, Germany

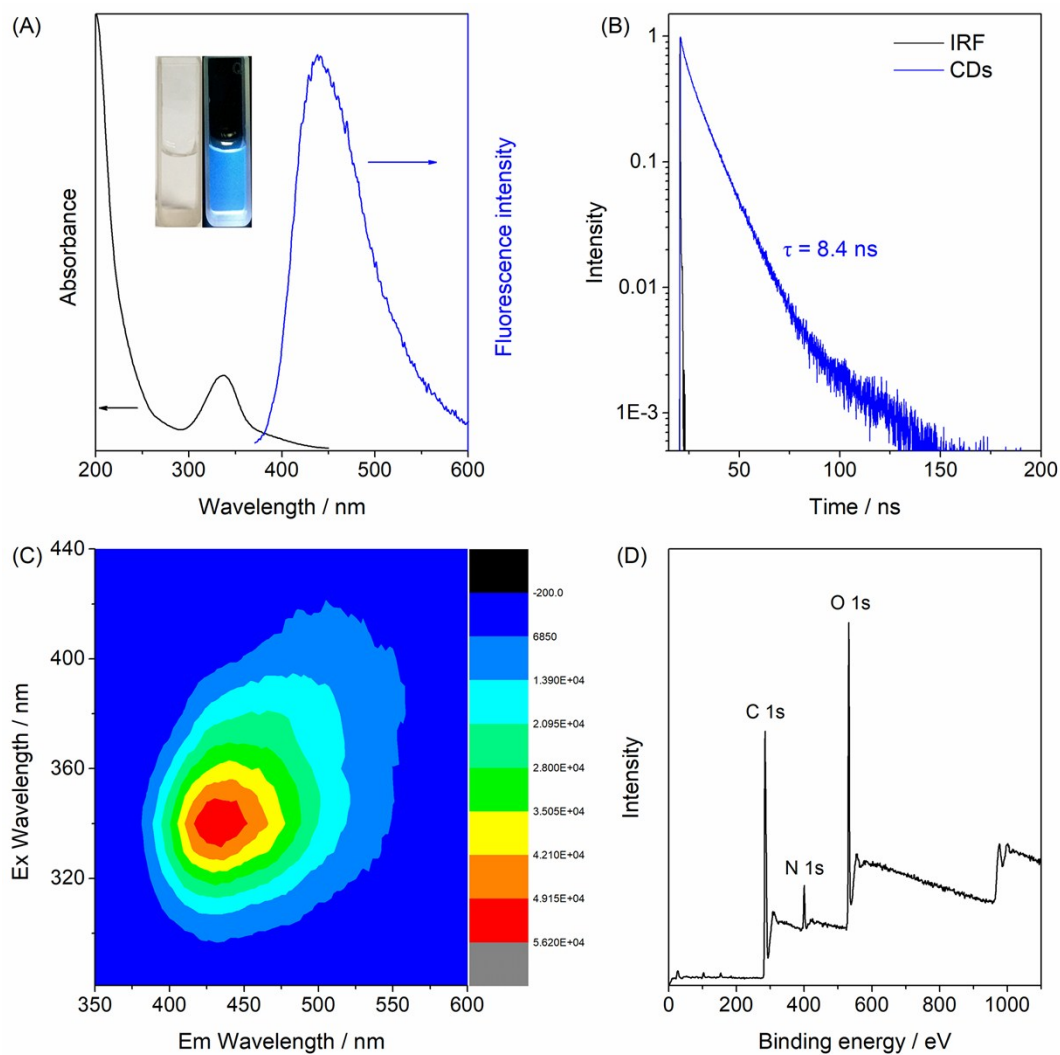


Figure S1. Characterization of CDs_{1:0.25}: (A) UV-vis absorption and fluorescence emission spectra (the inset is the photographs of CDs in ambient light (left) and under UV irradiation (right)); (B) fluorescence lifetime; (C) 3D fluorescence spectra; and (D) XPS spectra.

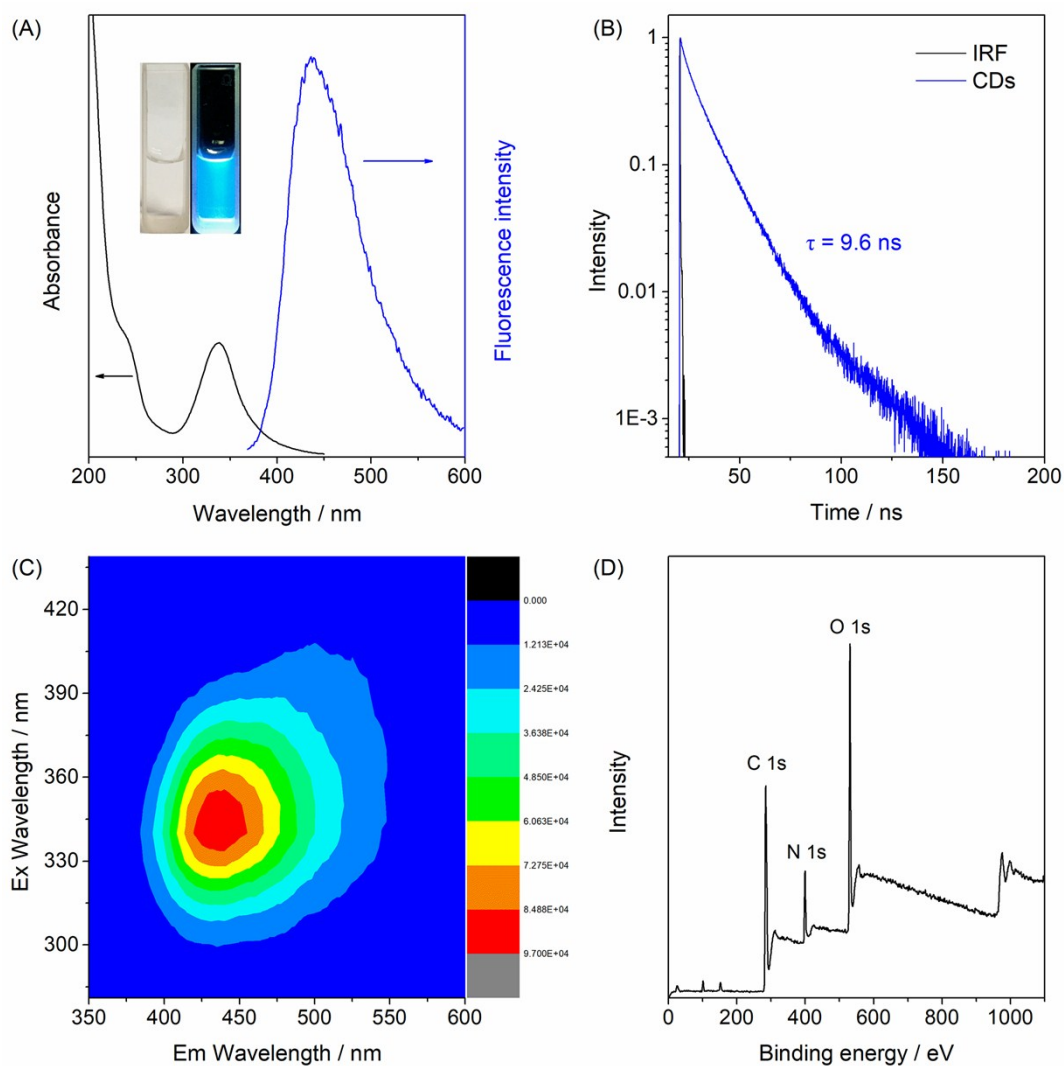


Figure S2. Characterization of CDs_{1:0.5}: (A) UV-vis absorption and fluorescence emission spectra (the inset is the photographs of CDs in ambient light (left) and under UV irradiation (right)); (B) fluorescence lifetime; (C) 3D fluorescence spectra; and (D) XPS spectra.

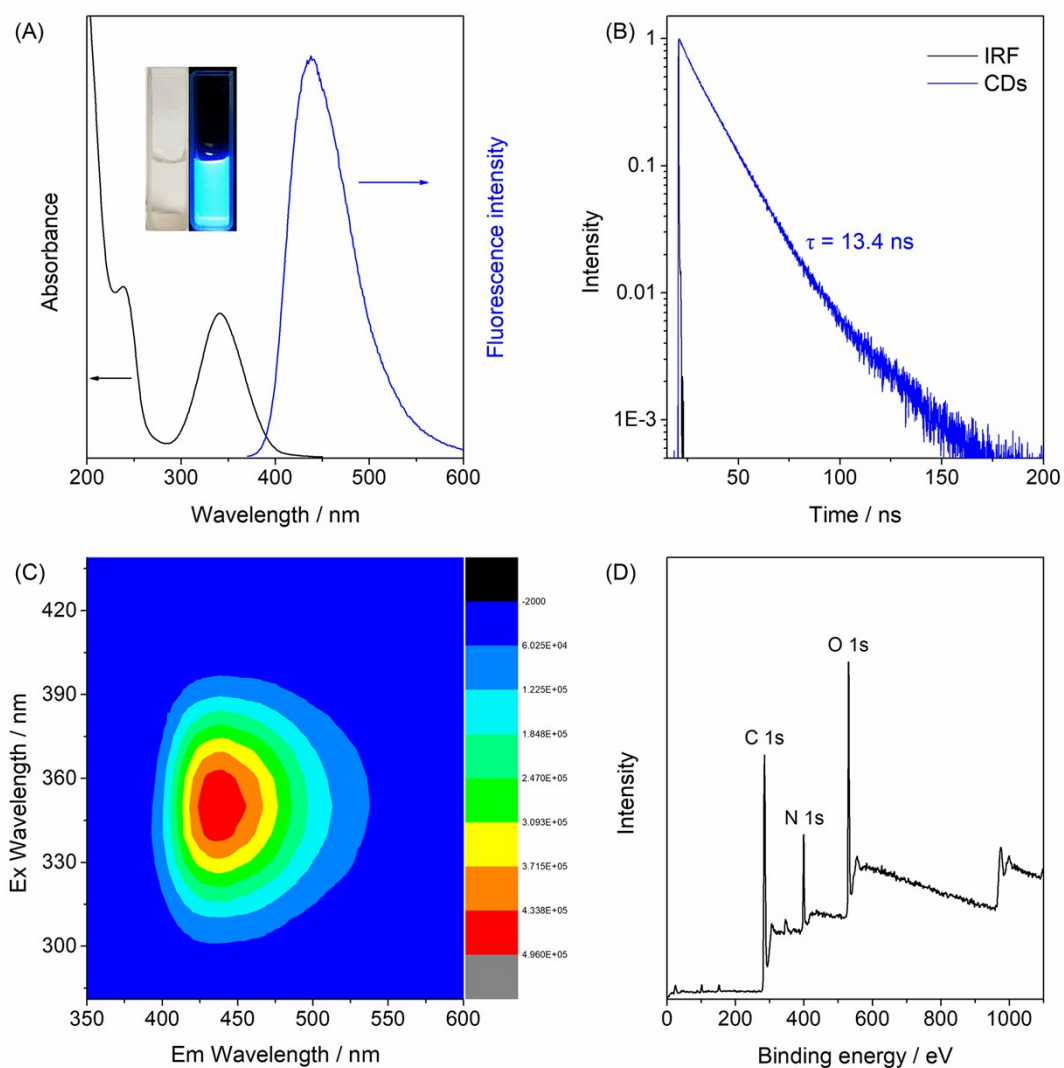


Figure S3. Characterization of CDs_{1:1}: (A) UV-vis absorption and fluorescence emission spectra (the inset is the photographs of CDs in ambient light (left) and under UV irradiation (right)); (B) fluorescence lifetime; (C) 3D fluorescence spectra; and (D) XPS spectra.

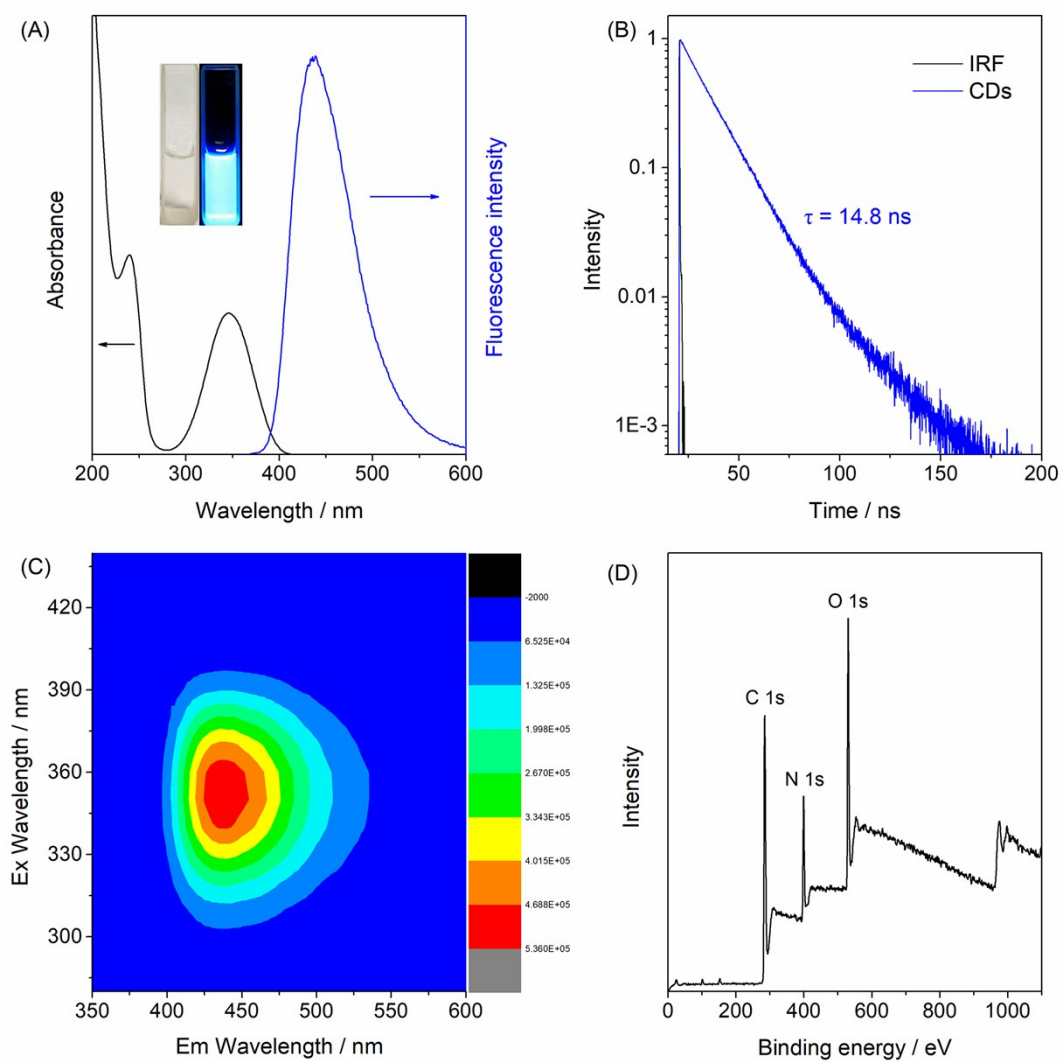


Figure S4. Characterization of CDs_{1:1.5}: (A) UV-vis absorption and fluorescence emission spectra (the inset is the photographs of CDs in ambient light (left) and under UV irradiation (right)); (B) fluorescence lifetime; (C) 3D fluorescence spectra; and (D) XPS spectra.

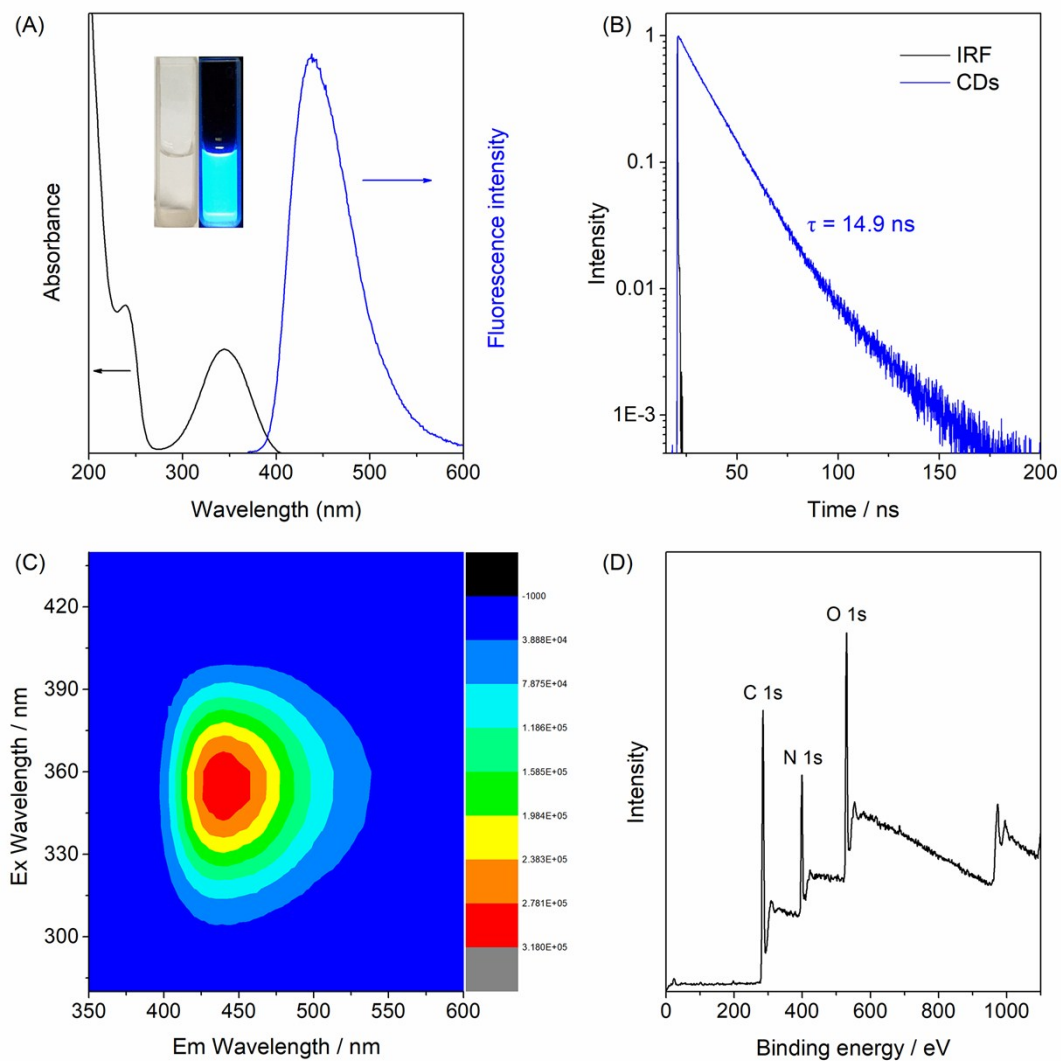


Figure S5. Characterization of CDs_{1:3}: (A) UV-vis absorption and fluorescence emission spectra (the inset is the photographs of CDs in ambient light (left) and under UV irradiation (right)); (B) fluorescence lifetime; (C) 3D fluorescence spectra; and (D) XPS spectra.

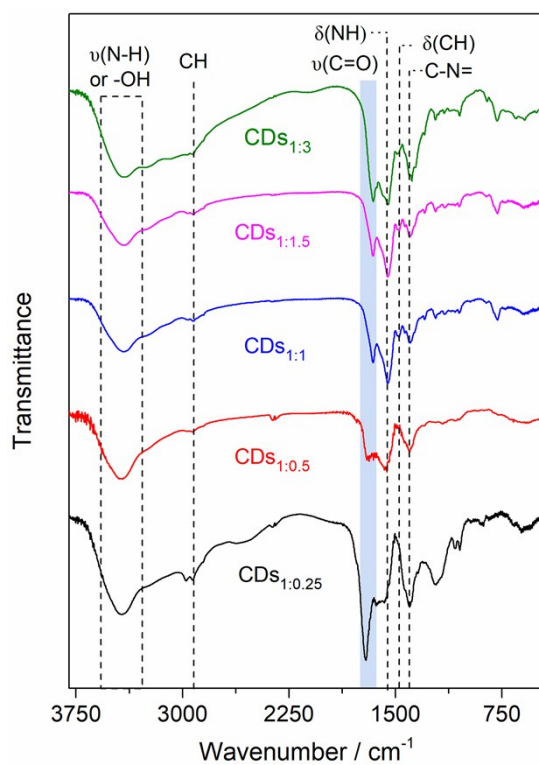


Figure S6. FT-IR spectra of CDs_{1:0.25} - CDs_{1:3}.

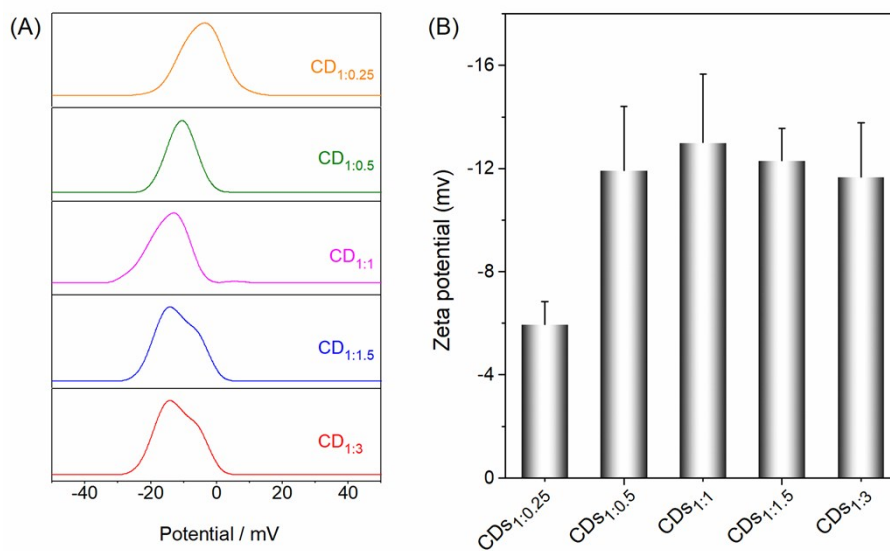


Figure S7. Zeta potentials of CDs_{1:0.25} - CDs_{1:3}.

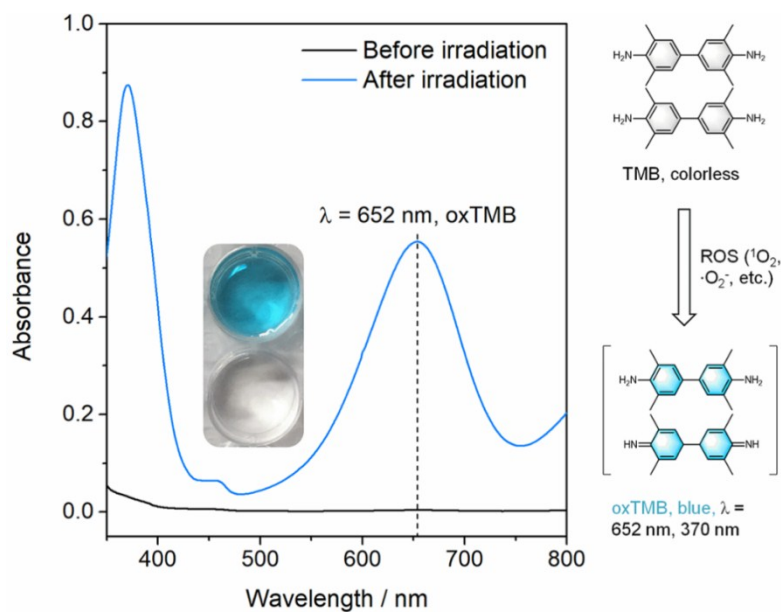


Figure S8. Absorption spectra of TMB before and after photosensitized oxidation mediated by N-CDs.

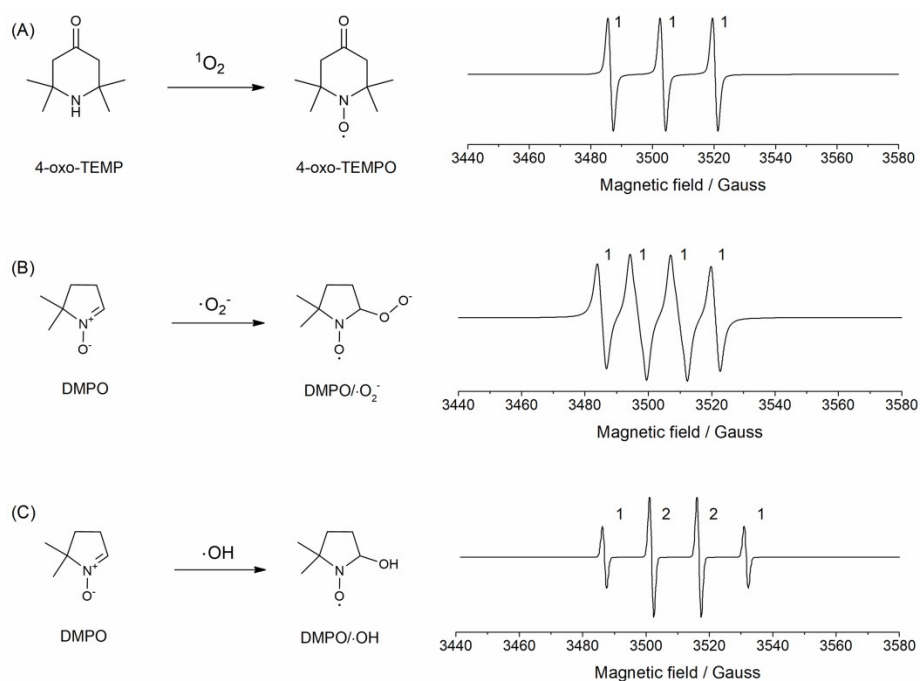


Figure S9. EPR trapping mechanisms for $^1\text{O}_2$ (A), $\cdot\text{O}_2\cdot$ (B), and $\cdot\text{OH}$ (C).

Table S2. The distribution of C, N, O element content in the XPS spectra of CDs_{1:0.25} - CDs_{1:3}.

Carbon dots	C (%)	N (%)	O (%)
CDs _{1:0.25}	73.6	5.4	21.0
CDs _{1:0.5}	68.9	9.4	21.7
CDs _{1:1}	70.7	10.7	18.6
CDs _{1:1.5}	69.7	13.3	17.0
CDs _{1:3}	67.2	16.0	16.8

Table S3. Singlet and triplet energy levels (unit: eV) of different Nitrogen doping type of Model one. For simplicity, graphitic, pyridinic, pyrrolic N was named as g, pd, and pl, respectively.

C-g		C-pd		C-pl		P-g		P-pd		P-pl	
S ₁ -S ₁₀	T ₁ -T ₁₀	S ₁ -S ₁₀	T ₁ -T ₁₀	S ₁ -S ₁₀	T ₁ -T ₁₀	S ₁ -S ₁₀	T ₁ -T ₁₀	S ₁ -S ₁₀	T ₁ -T ₁₀	S ₁ -S ₁₀	T ₁ -T ₁₀
2.6183	2.0943	2.9430	2.2937	3.0943	2.300	2.2303	1.6326	2.7324	1.9325	3.4047	2.2302
2.6774	2.1892	3.1302	2.5396	3.2251	2.8106	3.1097	2.0364	3.3638	2.3124	3.5861	3.2278
3.2720	2.5406	3.5405	2.7105	3.7220	2.8767	3.3826	2.6512	3.8326	3.2659	4.0371	3.3543
3.3448	2.7869	3.5890	2.9226	3.7334	2.9838	4.1129	3.3182	4.0379	3.3348	4.3133	3.5431
3.6554	3.0586	3.7668	3.1704	3.9944	3.4315	4.1276	3.4515	4.1126	3.4057	4.4142	3.6285
3.6964	3.1009	3.9531	3.2594	4.1349	3.5103	4.2171	3.5799	4.1977	3.6432	4.5801	3.7435
3.8317	3.2225	3.9983	3.3879	4.2226	3.6505	4.4498	3.6526	4.2537	3.7548	4.6229	4.1091
3.9226	3.3290	4.0568	3.5045	4.2678	3.8105	4.5742	4.0031	4.5063	3.8151	4.6503	4.3312
3.9482	3.4470	4.0701	3.5498	4.3309	3.8885	4.6752	4.1620	4.5961	4.0607	4.8339	4.3791
3.9876	3.5052	4.1145	3.6871	4.4496	3.9279	4.8384	4.3256	4.7110	4.2841	4.9205	4.5104

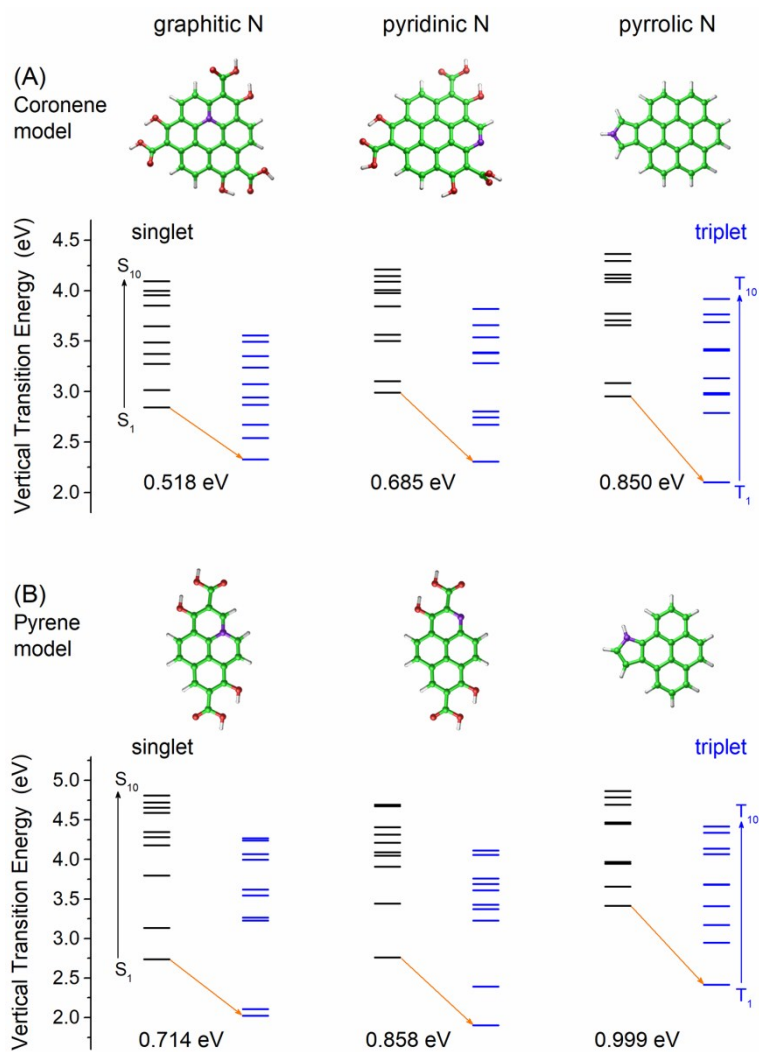


Figure S10. Singlet and triplet energy levels of coronene (A) and pyrene (B) models containing graphitic, pyridinic, and pyrrolic N structures. Notice: the position of the nitrogen atom was changed in each structure and the detailed data information was given in Table S4.

Table S4. Singlet and triplet energy levels (unit: eV) of different nitrogen doping type of Model two. For simplicity, graphitic, pyridinic, pyrrolic N were named as g, pd, and pl, respectively.

C-g-1		C-pd-1		C-pl-1		P-g-1		P-pd-1		P-pl-1	
S ₁ -S ₁₀	T ₁ -T ₁₀	S ₁ -S ₁₀	T ₁ -T ₁₀	S ₁ -S ₁₀	T ₁ -T ₁₀	S ₁ -S ₁₀	T ₁ -T ₁₀	S ₁ -S ₁₀	T ₁ -T ₁₀	S ₁ -S ₁₀	T ₁ -T ₁₀
2.8435	2.3252	2.9901	2.3053	2.9533	2.1029	2.7359	2.0223	2.7585	1.9010	3.4139	2.4151
3.0171	2.5418	3.1035	2.6723	3.0849	2.7896	3.1370	2.1067	3.4416	2.3943	3.6561	2.9449
3.2748	2.6726	3.500	2.7439	3.6582	2.9719	3.7962	3.2268	3.9057	3.2261	3.9442	3.1741
3.3735	2.8683	3.5642	2.8043	3.7060	2.9845	4.1784	3.2648	4.0505	3.3734	3.9700	3.4094
3.4852	2.9393	3.8481	3.2808	3.7742	3.1324	4.2847	3.5449	4.0890	3.4292	4.4509	3.6807
3.6496	3.0724	3.9765	3.3818	4.0856	3.4060	4.3474	3.6168	4.2115	3.6075	4.4684	3.6826
3.8549	3.2372	4.0059	3.3883	4.1246	3.4194	4.5916	3.9957	4.3149	3.6887	4.6926	4.0655
3.9578	3.3488	4.0899	3.5386	4.1612	3.6890	4.6523	4.0688	4.4089	3.7578	4.7855	4.1365
4.0005	3.4940	4.1454	3.6585	4.2962	3.7640	4.7182	4.2389	4.6750	4.0605	4.7862	4.3370
4.0962	3.5560	4.2113	3.8193	4.3660	3.9189	4.8080	4.2681	4.6891	4.1118	4.8652	4.4181

Table S5. The oscillator strengths of different nitrogen doping types.

	S ₁	S ₂	S ₃	S ₄	S ₅	S ₆	S ₇	S ₈	S ₉	S ₁₀
C-g	0.0811	0.1164	0.1932	0.2700	0.0652	0.1204	0.1822	0.1960	0.0957	0.5824
C-pd	0.0786	0.0046	0.7280	0.7327	0.2102	0.0628	0.0326	0.0314	0.0059	0.0067
C-pl	0.0131	0.0416	0.8503	0.5318	0.0216	0.0894	0.1158	0.01177	0.0040	0.1534
C-g-1	0.0631	0.0125	0.0462	0.4275	0.4083	0.2492	0.0376	0.2338	0.1644	0.0507
C-pd-1	0.0157	0.0611	0.6283	0.8125	0.0741	0.0068	0.0046	0.0119	0.0131	0.0318
C-pl-1	0.1166	0.0113	0.7084	0.0003	0.0591	0.3463	0.0220	0.2008	0.2235	0.2377
P-g	0.0813	0.0951	0.2346	0.1130	0.1401	0.8624	0	0	0.1256	0.0072
P-pd	0.1570	0.2385	0.0105	0.0002	0.0005	0.0003	0.8728	0.0005	0.7899	0.0022
P-pl	0.2510	0.0200	0.3105	0.0524	0.0311	0.2863	0.0782	0.0050	0.0944	0.0017
P-g-1	0.0958	0.03017	0.0069	0.3761	0.0332	0.4300	0.0206	0	0.1682	0.2156
P-pd-1	0.2150	0.2156	0.0026	0.0010	0.0002	0.6521	0.0063	0.2099	0.5651	0.2071
P-pl-1	0.0353	0.1369	0.1926	0.2681	0.0921	0.0038	0.0077	0	0.0374	0.0274

Table S6. Absorption wavelengths corresponding to the maximum allowable transition (oscillator strength) of the considered models.(agreed well with the obtained absorption profiles of N-CDs)

Coronene model	C-g	C-pd	C-pl	C-g-1	C-pd-1	C-pl-1
λ (nm)	378.92	345.46	333.11	367.53	347.86	338.92
Pyrene model	P-g	P-pd	P-pl	P-g-1	P-pd-1	P-pl-1
λ (nm)	294.00	291.48	307.12	285.19	294.39	312.30

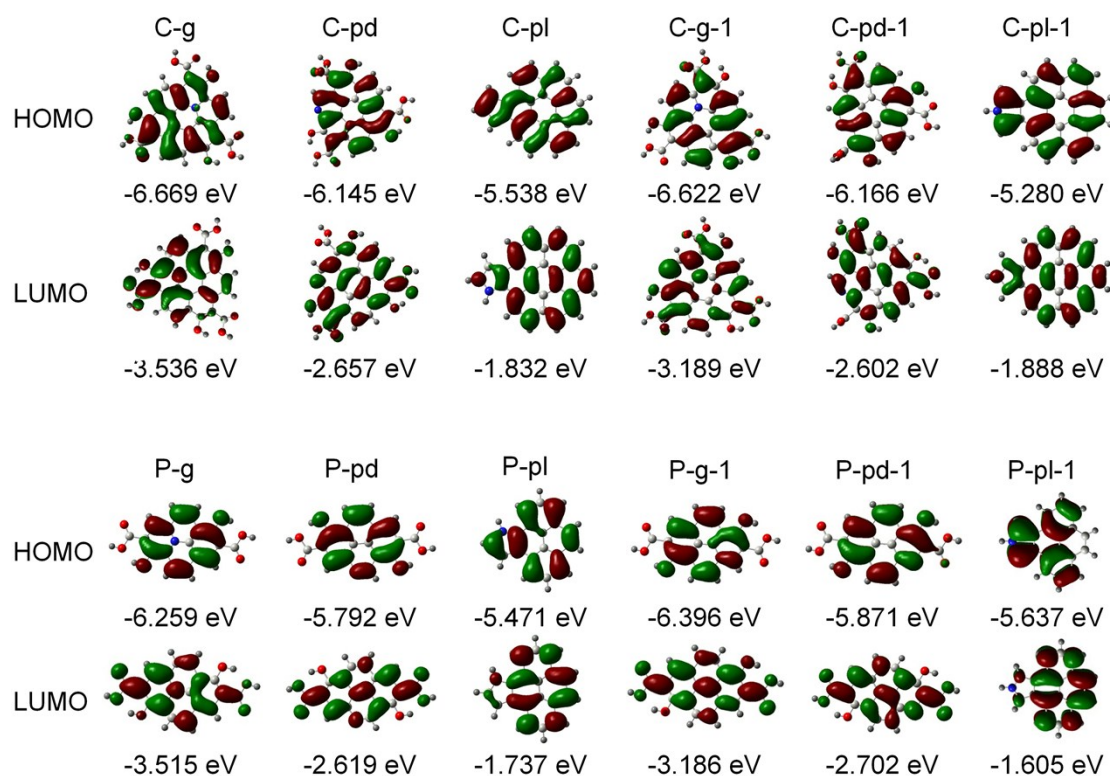


Figure S11. Orbital information of different nitrogen doping types.

Re-confirmation of the theoretical model for calculation of ΔE_{ST} of N-CDs. Since coronene and pyrene doped by single graphitic N (replacing one C atom by N) are doublet electronic state, the graphitic N structure was changed from an electrically neutral doublet state to a singlet state with a positive charge in the text. To further confirm the calculation results, the graphitic N structures were inserted with two N atoms for neutralizing the singlet ground states. As can be seen from Figure S12, graphitic N still exhibited the lowest ΔE_{ST} value in both the coronene and pyrene models (graphitic N < pyridinic N < pyrrolic N), which is consistent with the results obtained by those containing single N atom (a singlet state with a positive charge).

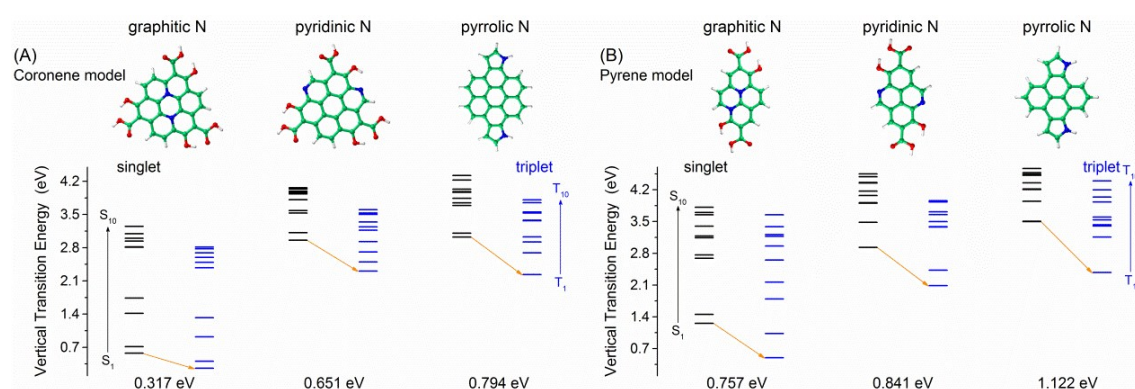


Figure S12. Singlet and triplet energy levels of coronene (A) and pyrene (B) models containing graphitic, pyridinic, and pyrrolic N structures (with two N atoms).

Table S7. Oxygen adsorption calculation of different nitrogen-doped types (unit: eV).

	$E_{N\text{-doping}+O_2}$	E_{total}	E_{ads}
c-g	-51163.8178	-51162.4310	-1.3868
c-g-1	-51163.9507	-51162.4739	-1.4768
c-pd	-51152.2163	-51150.9809	-1.2354
c-pd-1	-51152.3221	-51151.0531	-1.2690
c-pl	-32759.7789	-32758.8518	-0.9272
c-pl-1	-32759.5549	-32759.7448	0.1899
p-g	-35654.3442	-35652.9526	-1.3916
p-g-1	-35654.6016	-35653.2382	-1.3634
p-pd	-35642.9603	-35641.6826	-1.2777
p-pd-1	-35642.9021	-35641.7679	-1.1342
p-pl	-24428.9214	-24428.2171	-0.7043
p-pl-1	-24428.9214	-24429.0006	0.0792

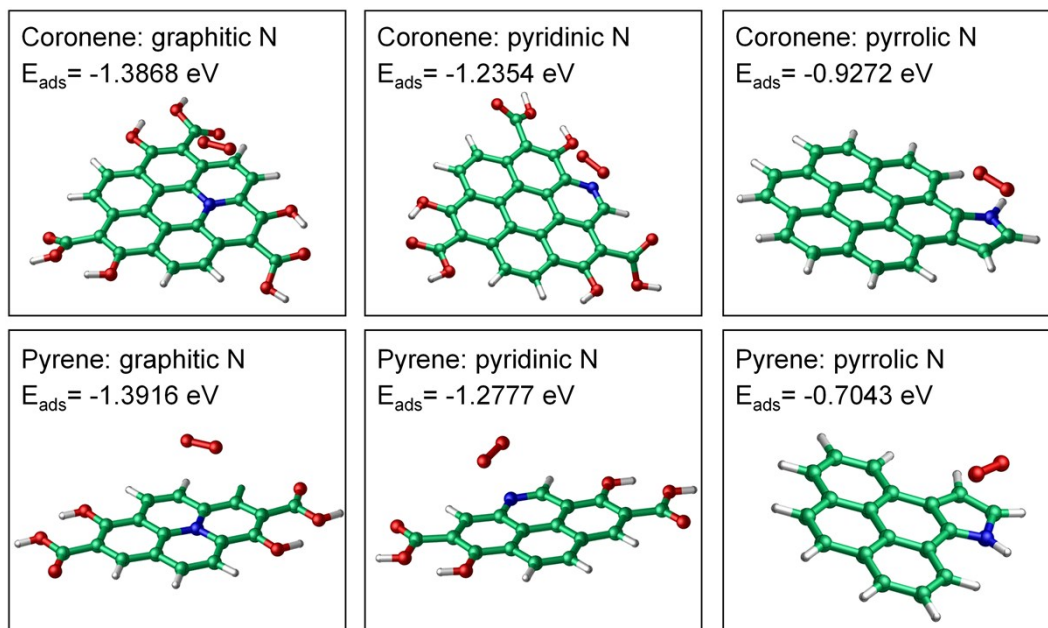


Figure S13. Oxygen adsorption calculation based on different nitrogen doping types of pyrene and coronene. Here, we add a DFT-D3 dispersion correction method, in which each model is first subjected to geometric optimization and frequency analysis to obtain its optimized configuration, and then use the optimized configuration to calculate the oxygen adsorption. Besides, the graphitic N structures were also changed from an electrically neutral doublet state to a singlet state with a positive charge as those in Figure 5.

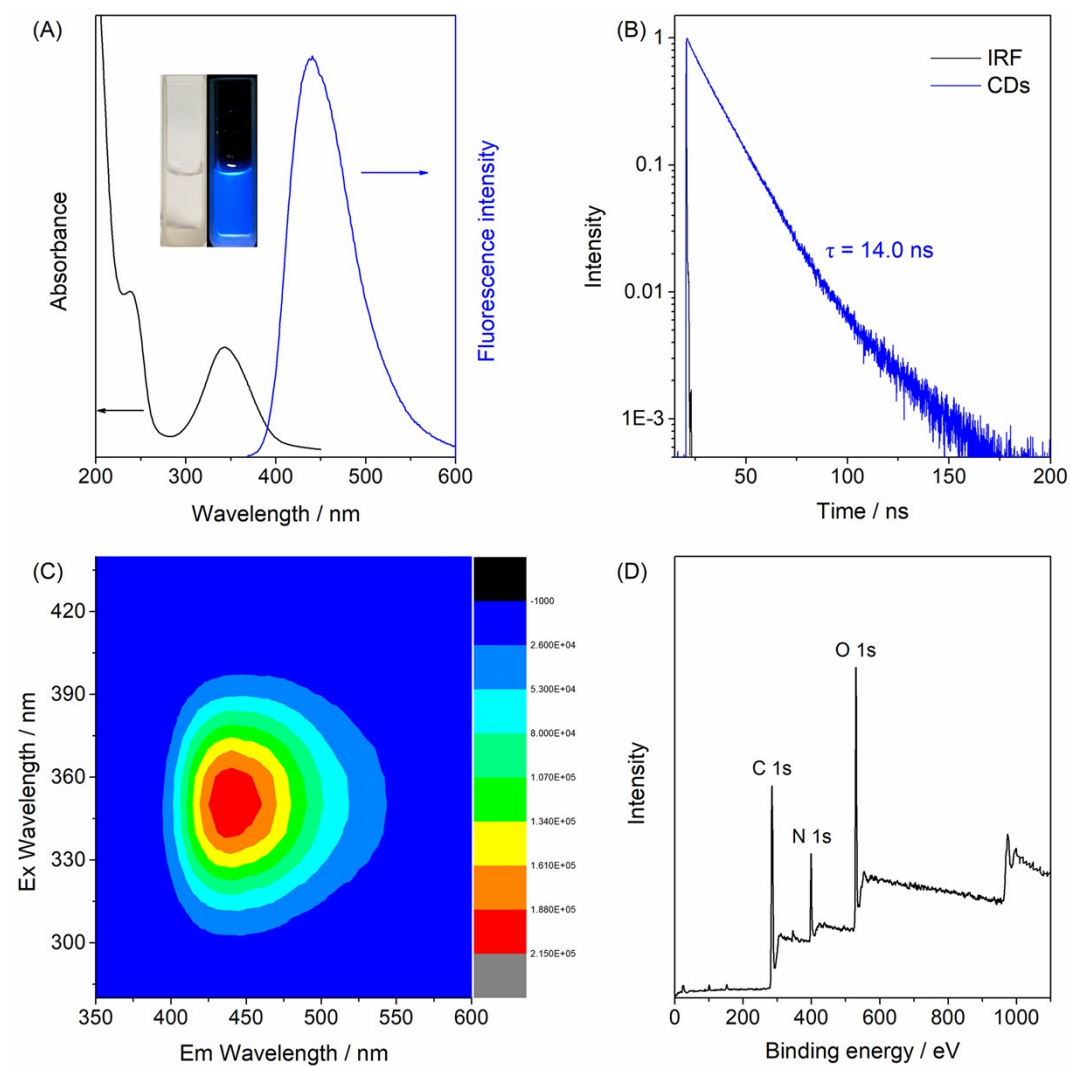


Figure S14. Characterization of CDs_{150°C}: (A) UV-vis absorption and fluorescence emission spectra (the inset is the photographs of CDs in ambient light (left) and under UV irradiation (right)); (B) fluorescence lifetime; (C) 3D fluorescence spectra; and (D) XPS spectra.

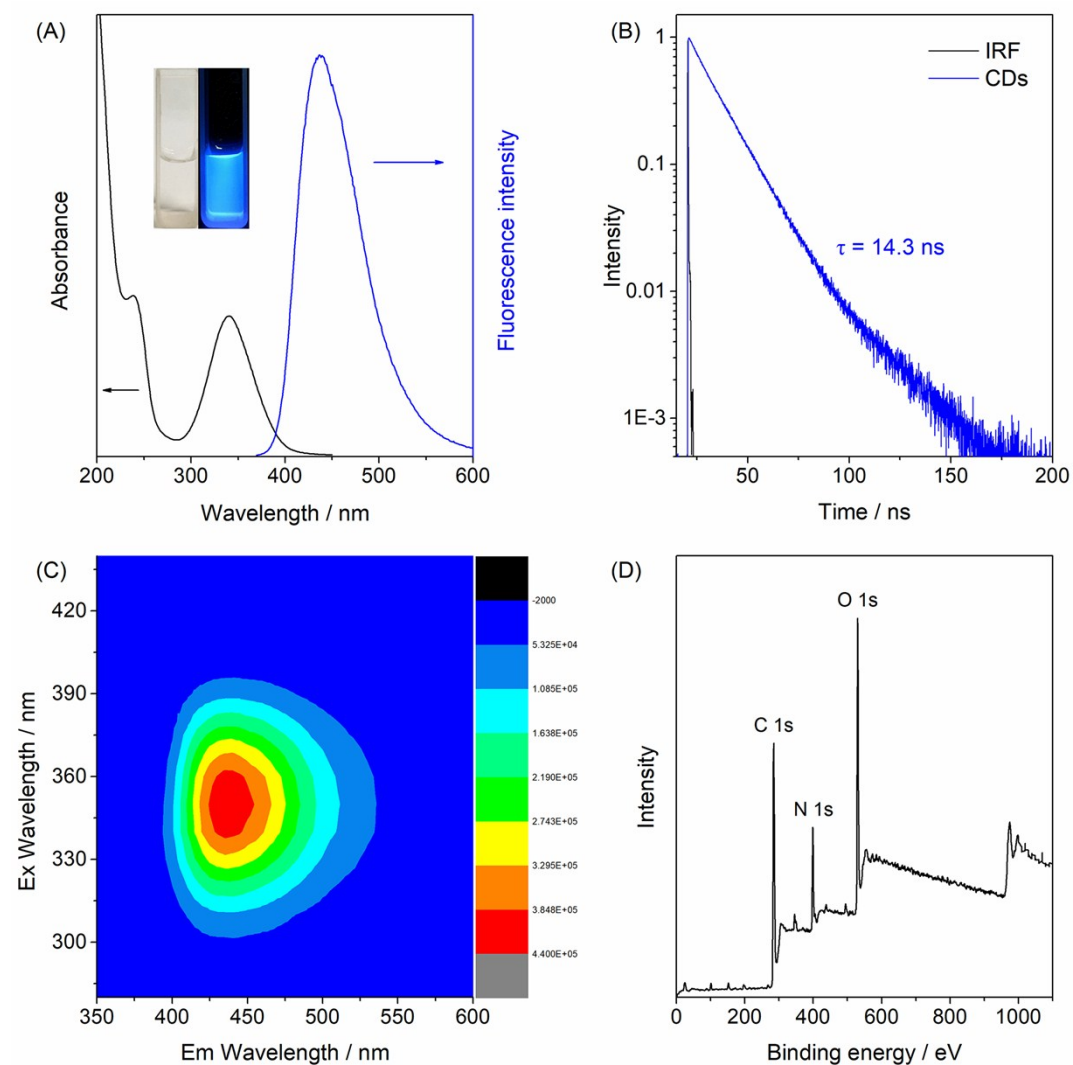


Figure S15. Characterization of CDs_{180°C}: (A) UV-vis absorption and fluorescence emission spectra (the inset is the photographs of CDs in ambient light (left) and under UV irradiation (right)); (B) fluorescence lifetime; (C) 3D fluorescence spectra; and (D) XPS spectra.

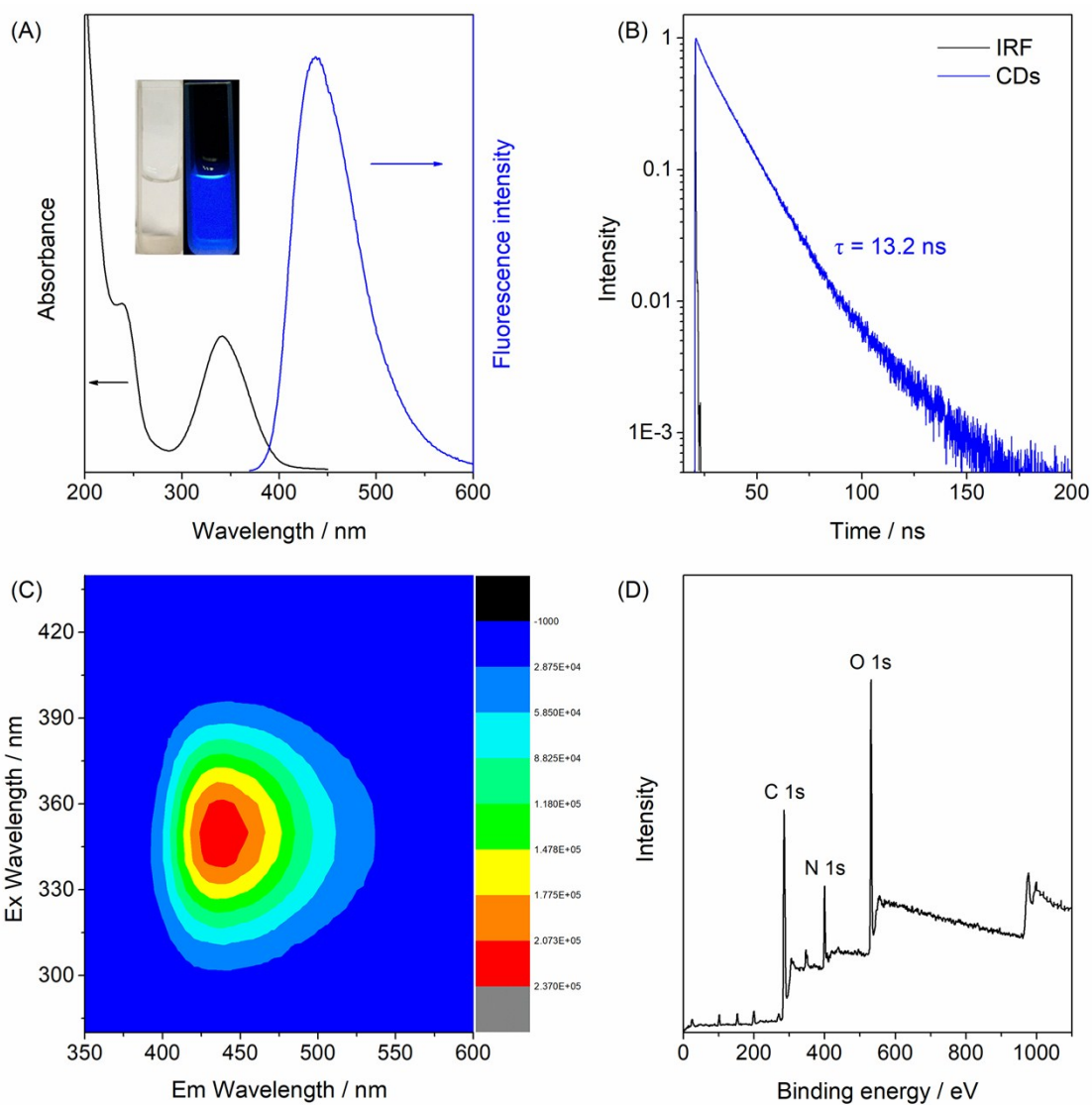


Figure S16. Characterization of CDs₂₁₀°C: (A) UV-vis absorption and fluorescence emission spectra (the inset is the photographs of CDs in ambient light (left) and under UV irradiation (right)); (B) fluorescence lifetime; (C) 3D fluorescence spectra; and (D) XPS spectra.

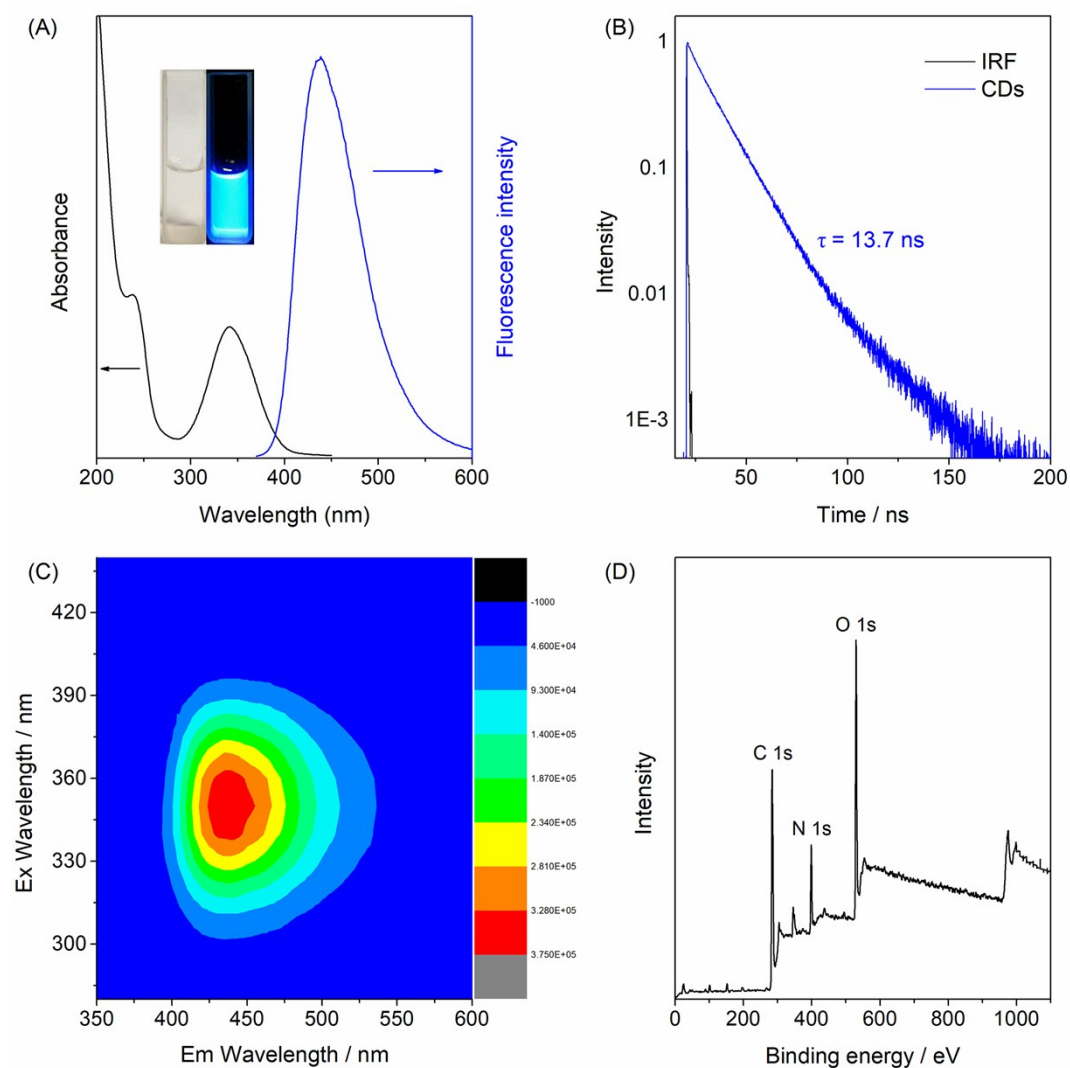


Figure S17. Characterization of CDs_{240°C}: (A) UV-vis absorption and fluorescence emission spectra (the inset is the photographs of CDs in ambient light (left) and under UV irradiation (right)); (B) fluorescence lifetime; (C) 3D fluorescence spectra; and (D) XPS spectra.

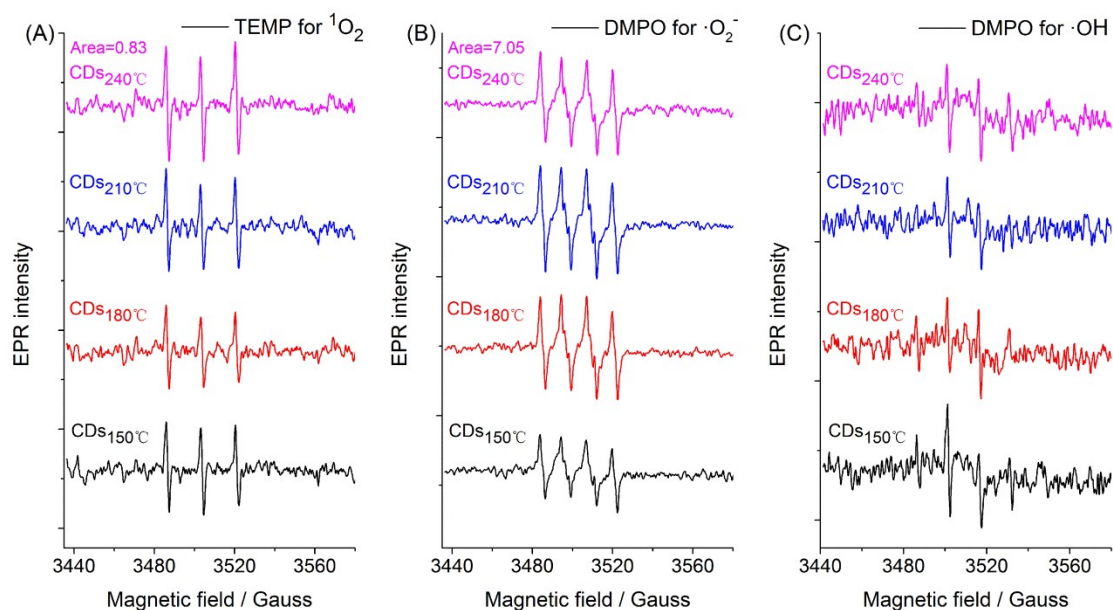


Figure S18. EPR characterizations of the photosensitized generation of ROSs from CDS_{150°C}-CDS_{240°C}: (A) TEMP for $^1\text{O}_2$; (B) DMPO for $\cdot\text{O}_2^-$ (in DMSO); and (C) DMPO for $\cdot\text{OH}$ (in water).

Table S8. The distribution of C, N, O element content in the XPS spectrum of CDS_{150°C} - CDS_{240°C}.

Carbon dots	C (%)	N (%)	O (%)
CDS _{150°C}	65.9	11.8	22.3
CDS _{180°C}	65.3	12.6	22.1
CDS _{210°C}	64.9	11.6	23.5
CDS _{240°C}	65.9	10.7	23.4

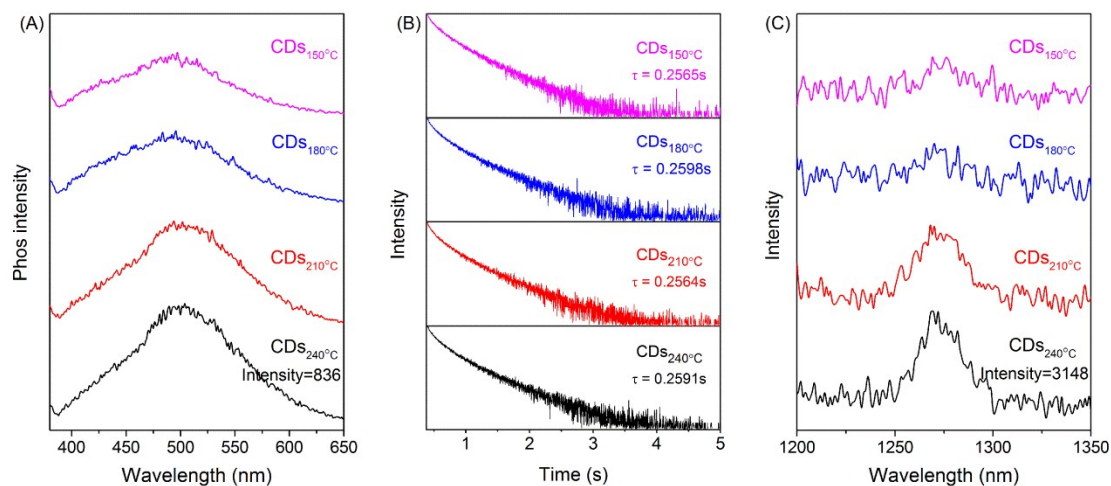


Figure S19. Evidences for activation of the triplet states of N-CDs (from $\text{CDs}_{150^\circ\text{C}}$ to $\text{CDs}_{240^\circ\text{C}}$): (A) phosphorescence emission spectra of N-CDs embedded in PVA composite film ($\lambda_{\text{EX}} = 365$ nm, flash lamp, delay time of 1 ms); (B) phosphorescence lifetime of N-CDs embedded in PVA composite film ($\lambda_{\text{EX}} = 355$ nm, SpectraLED); and (C) characterized $^1\text{O}_2$ phosphorescence emission spectra of the N-CDs in the $\text{CD}_3\text{CN}-\text{D}_2\text{O}$ mixed solvent ($v/v = 15/1$, $\lambda_{\text{EX}} = 365$ nm).

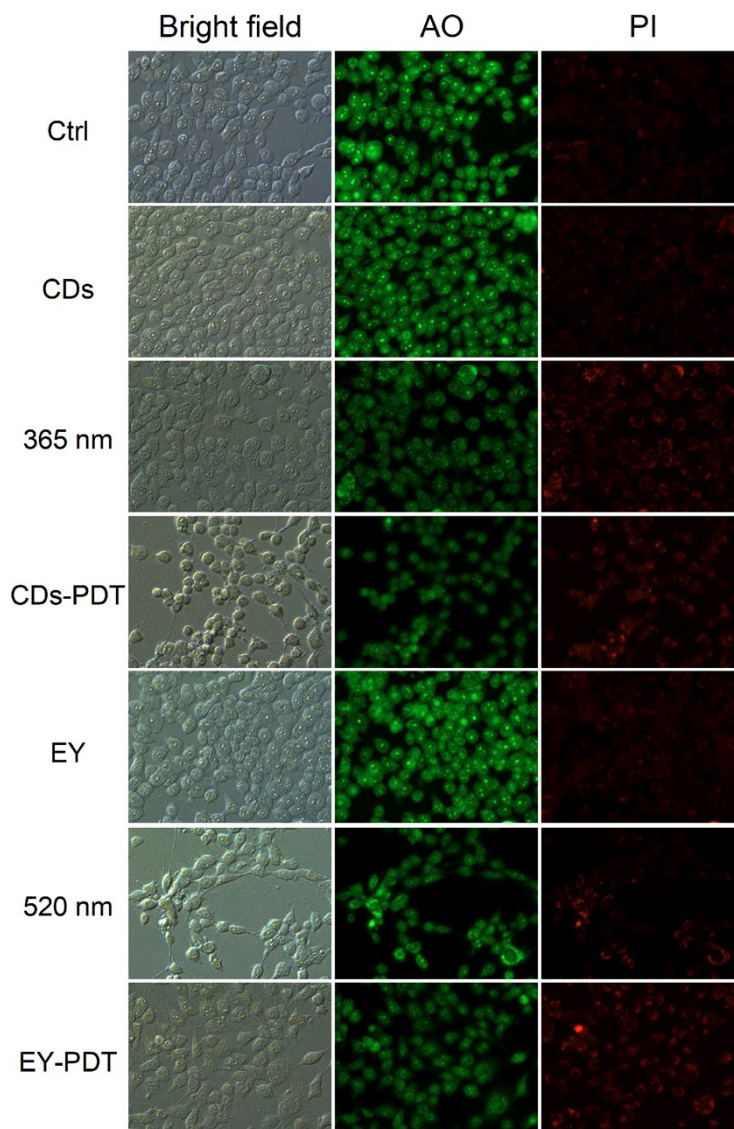


Figure S20. Live/Dead cells staining of N-CDs and eosin Y-treated 4T1 cells with acridine orange-sodium propidate (AO/PI) kit.

Detection of ROS in 4T1 cells. 4T1 cells incubated in a 12-well plate were divided into four groups, and no other treatment was used as a control in the first group. In the second group, 4T1 cells were irradiated with 365 nm LED lamps, and the third group was only incubated with 4T1 and N-CDs. In the last group, 4T1 cells were co-incubated with N-CDs, and then subjected to light irradiation to perform a PDT process, and PBS was washed twice. All samples were stained with the ROS

probe DCFH-DA and the nuclei were stained with Hoechst33342. The green fluorescence of DCFH-DA was subsequently observed with a fluorescence inverted microscope.

In vitro cytotoxicity assay. The cell viability was determined by cell counting kit-8 (CCK-8). Briefly, 100 μ L Dulbecco's modified Eagle's medium (DMEM) containing 1×10^4 4T1 cells were cultured per well of 96-well assay plates. After being cultured for 24 h (37 °C and 5% CO₂), new DMEM medium with various concentrations of N-CDs, EY were added to the wells and further cultured for 12 h. One plate was used for exploring the cytotoxicity of the N-CDs and EY without irradiation. The other two plates were respectively irradiated using ultraviolet light-emitting diode (LED) (N-CDs, $\lambda = 365$ nm, EY, $\lambda = 520$ nm) with an intensity of 25 J•cm⁻² for 5 min. Next, the medium was removed and washed with phosphate-buffered saline (PBS) three times. Then, 100 μ L CCK-8/DMEM mixture solution (v/v, 1/9) was added into each well for another 2 h incubation. The cell viability was determined through measuring the absorbance of each sample at 450 nm with a microplate reader.

AO/PI assay. Cell viability also was assessed by acridine orange-propidium iodide (AO/PI) staining. 4T1 cells were cultured in a 12-well plate according to the previous method. And then the 4T1 cells and working solution (AO: 670 μ M, PI: 750 μ M) were kept in dark at 4°C for 20 minutes for AO/PI staining. Finally, it was observed in a fluorescence inverted microscope in which living cells were green (AO) and dead cells were red (PI).

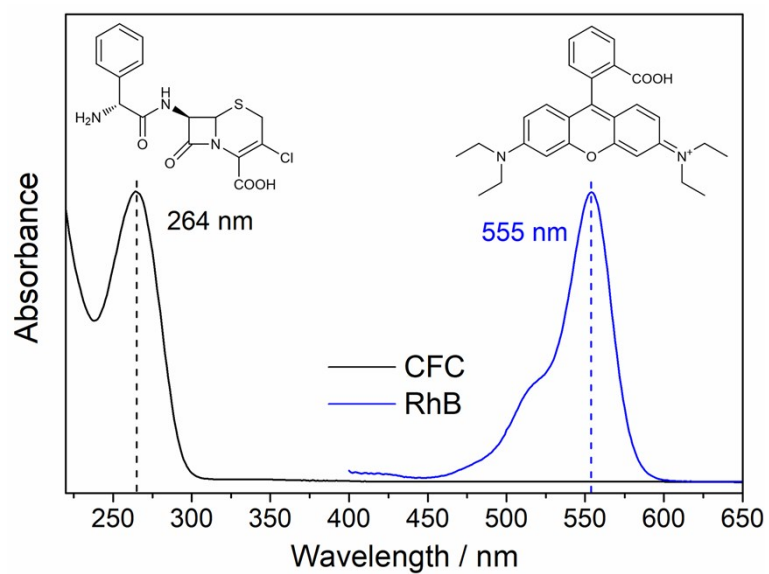


Figure S21. Absorption spectra of RhB and CFC.

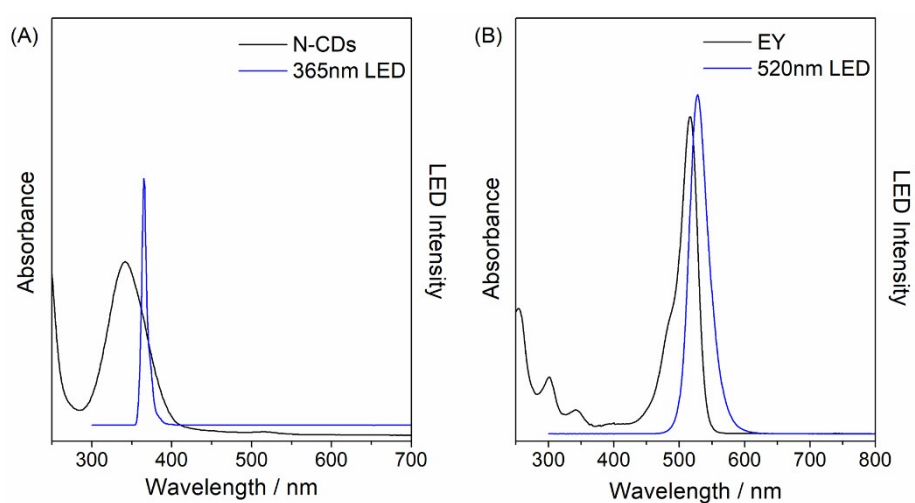


Figure S22. Absorption spectra of N-CDs and UV LED (A), and eosin Y and green LED (B).

Photosensitization of N-CDs for pollutant removal. The photosensitization experiments were evaluated by photodegradation of the cefaclor (CFC) and Rhodamine B (RhB) aqueous solution irradiated by a 365 nm LED (3 V, 3 W).

Typically, 5 mg/mL CD suspension (24 μ L) was uniformly dispersed with CFC (9.3 μ L) or RhB (7.6 μ L) in a cuvette containing 2 mL of deionized water. Subsequently, the above solution was irradiated with a 365 nm LED. At given time intervals, the supernatant was separated by centrifugation at 9 000 rpm for 5 min. Afterwards, 2 mL of supernatant was sampled and analyzed with a UV-visible spectrophotometer through the absorbance at 264 or 555 nm to monitoring the process of photosensitization. For comparison, traditional photosensitizer Eosin Y was used to evaluate the effect of N-CDs photosensitization. Similarly, repeat the above experiment by changing the CDs to EY (5 mg/mL, 2.6 μ L, 520 nm LED irradiation)